Supporting Information (SI)

Polyetherimide (PEI) nanocomposite with WS_2 nanotubes

Dotan Babai, Ido Pinkas, Reshef Tenne and Doron Naveh

SI_1. Material and synthesis methods

a. Figures of the inserted WS_2 INT

Fig. S1 displays high-resolution scanning electron microscopy (SEM) images of a pure phase of WS_2 nanotubes in two magnifications (a&b) and transmission electron microscopy (TEM) image of a multiwall WS_2 nanotube (c).

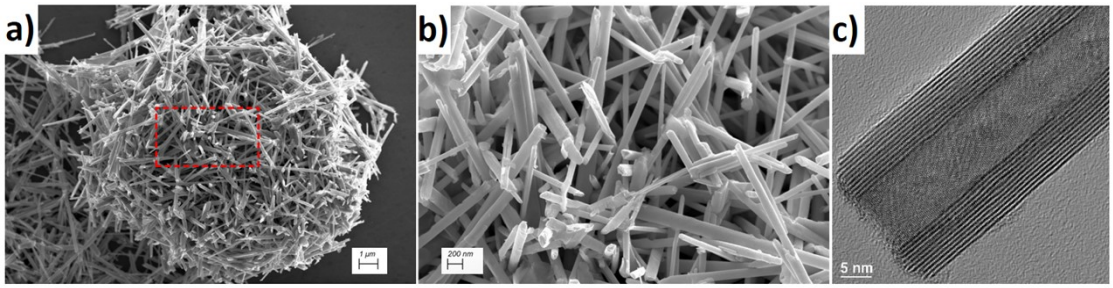

Fig. S1 - SEM and TEM images of WS_2 INTs employed in the study: (a) agglomerate of nanotubes, (b) enlarged view of the region marked by the red square, and (c) representative TEM image of a WS_2 nanotube.

b. Nanocomposite fabrication and dispersion methods of the WS_2 INT

Prior to the traction of nanocomposite filaments from the molten blend, considerable efforts were dedicated to the fabrication of nanocomposite foils using conventional solvent-based methods. Using ordinary known solvents, like chloroform and dimethyl ammonium chloride (DMA). Unfortunately, despite repeated attempts, the resulting nanocomposites displayed unsatisfactory mechanical properties, particularly in terms of reduced plasticity. SEM images analysis of dried specimens after tensile tests revealed cylindrical voids surrounding the nanotubes which were prepared according to this method.

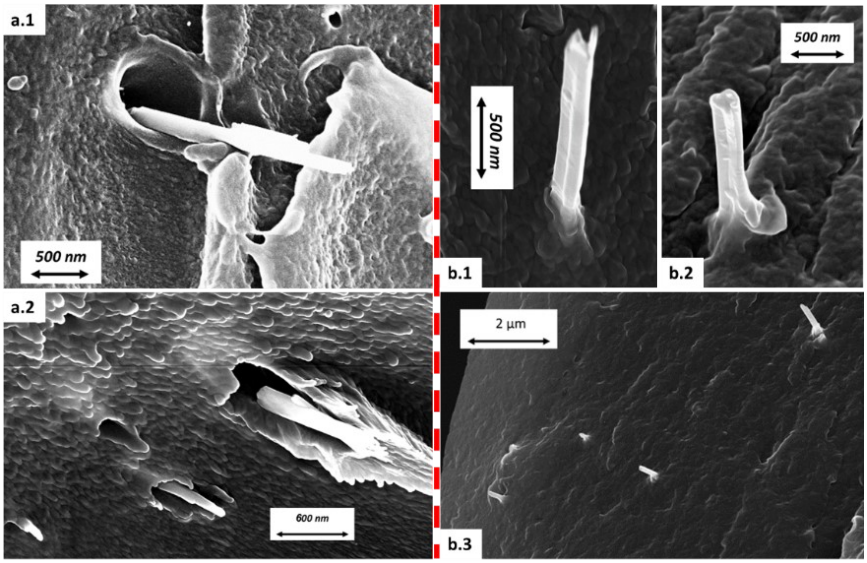

Fig. S2 - SEM images of truncated WS_2 nanotubes from post-failure nanocomposite (PEI+WS_2 INTs) filaments and strings. On the left, the surfaces of fractured PEI+ WS_2 INTs filaments prepared using DMA (Fig a.1) and chloroform (Fig a.2). On the right, images of fractured strings originating from a molten mix of PEI+WS_2 INT at 350 °C.

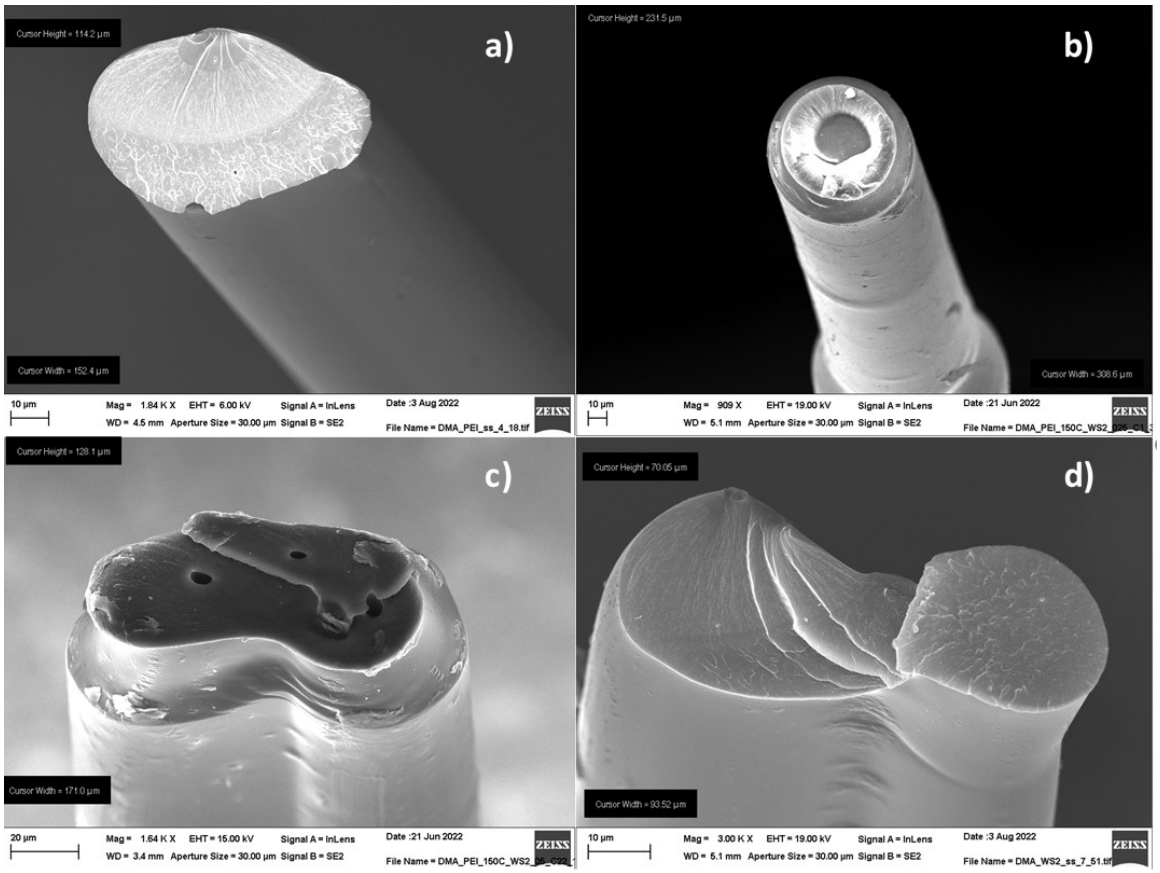

Fig. S3 - SEM images of post-failure nanocomposite strings. All strings were produced at 350 °C. The tensile tests of the strings were performed using the DMA-850 set-up. a) Pristine PEI string, b) PEI + 0.25 wt% WS_2 INT, c) PEI + 0.5 wt% WS_2 INT, d) PEI + 2 wt% WS_2 INT.

As ***Fig.* S3** demonstrates, the production of strings with nearly regular cross-sections is attainable. The necks observed in ***Fig.* S3*b-c*** were formed during a tensile test of the nanocomposite strings at 130 K (further details are available in the main text). The low-temperature environment restricted plastic deformation, resulting in rupture immediately after plastic yielding of the strings.

c. Truncated WS_2 nanotubes emanating from post-failure nanocomposite strings

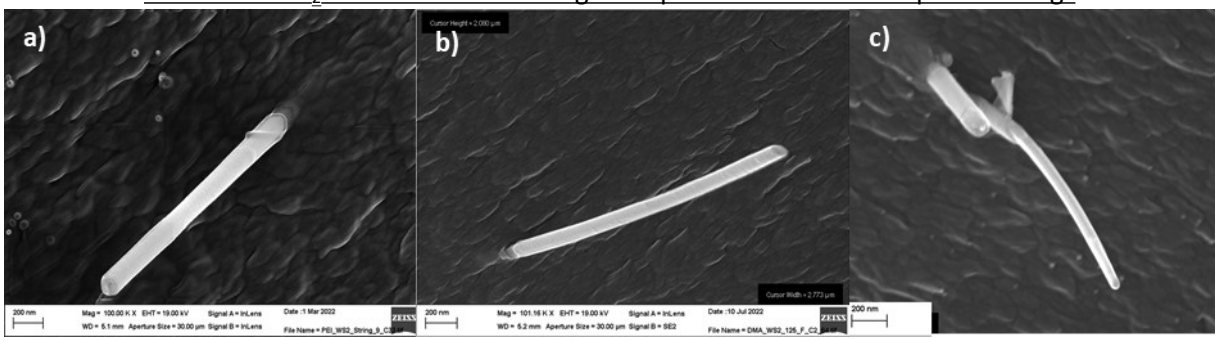

Fig. S4 - SEM images of fractured strings. Please note the sword in the sheath mode of failure of the nanotube on the right in (c).

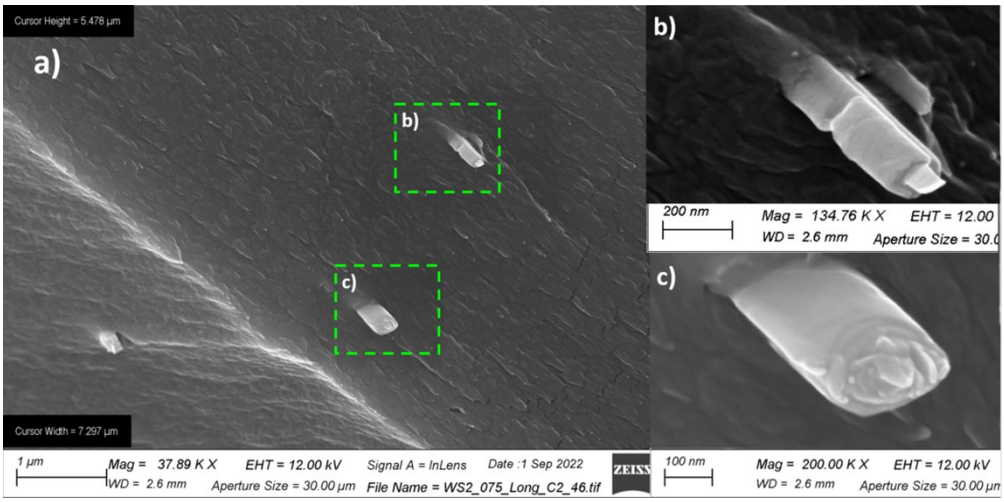

Fig. S5 - Series of SEM images for a fractured string of PEI+0.75 wt% INTs. Frames (b)-(c) show higher resolution images of the broken nanotubes fragments. The bright contrast in the center of the broken nanostructure is attributed to the nanotubes, which are conformably coated with a visibly darker polymer film.

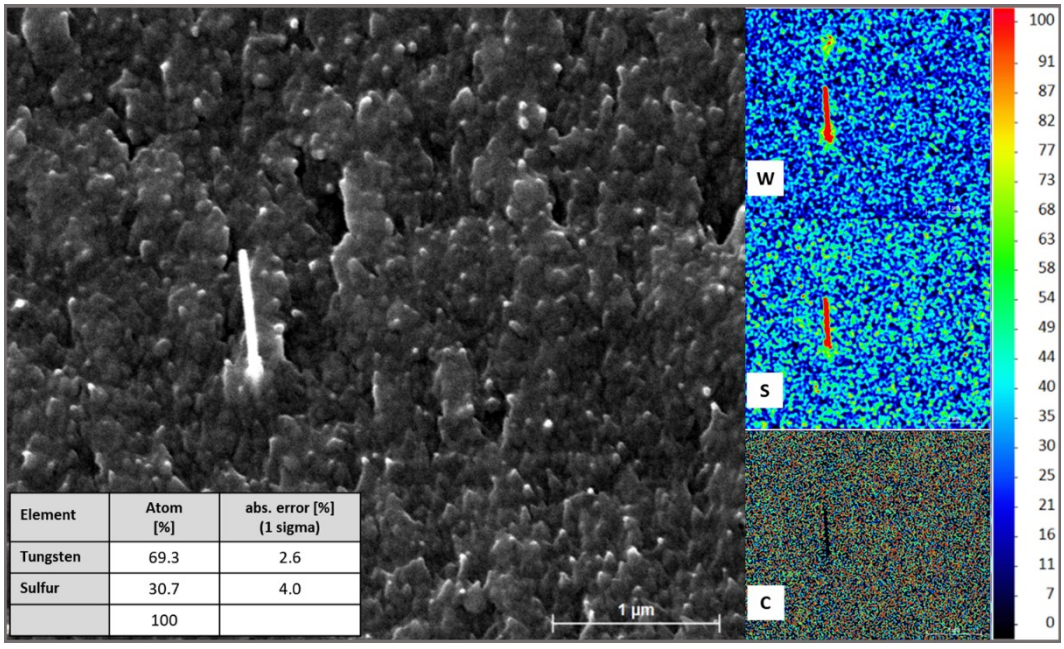

Element	Atom [%]	abs. error [%] (1 sigma)
Tungsten	69.3	2.6
Sulfur	30.7	4.0
	100	

Fig. S6 - SEM image of a truncated nanocomposite string with 2.0 wt% WS_2 INTs and the corresponding energy dispersive X-ray spectroscopy (EDS) maps of tungsten sulfur and carbon. The EDS results in the integrated table shows that the S/W atom ratio is 2.25.

SI_2. Measurements

a. Stress-Strain curves

The stress-strain tests were conducted with the cross-sectional area of the strings determined solely based on the measured diameters. Following the tensile tests and subsequent failure of the strings, the two halves were subjected to SEM analysis. They were positioned in parallel with the SEM beam to enable normal azimuth imaging of the fractured area. The SEM images facilitate scrutiny of the true cross-sectional area of the string after reaching the ultimate tensile strength (UTS). The stress-strain curves could then be plotted in ***Fig.* S7**, using the cross-sectional area, considering that the only truly known value of the cross-section area is at the UTS point.

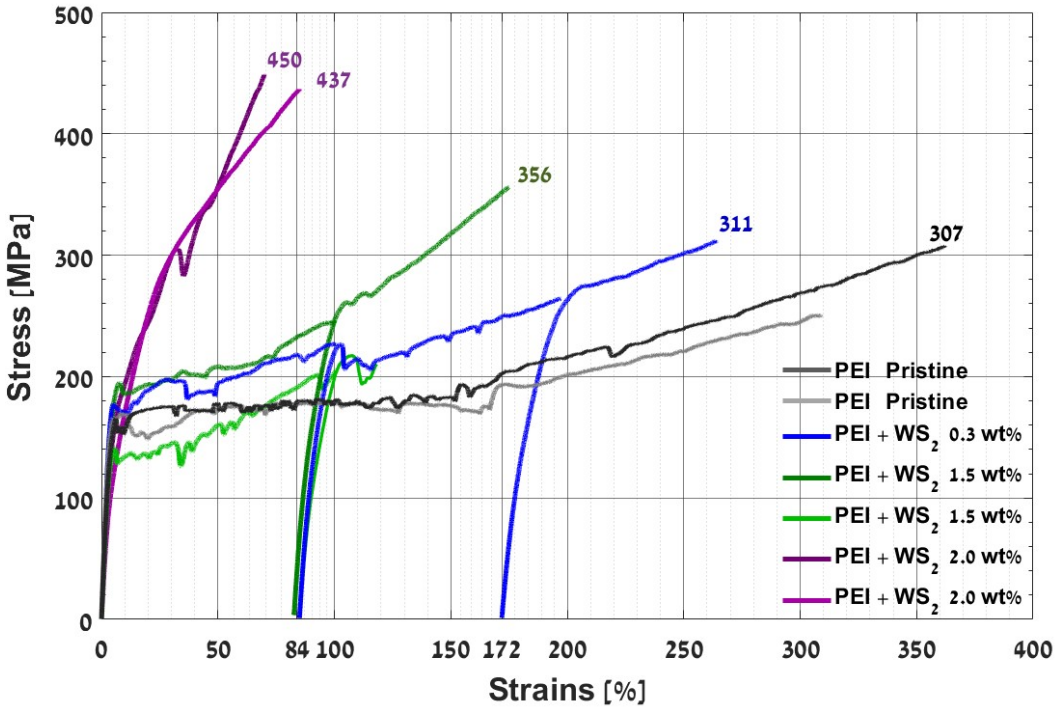

Fig. S7 - Stress-strain curves of nanocomposite strings calibrated by the true cross-section obtained by SEM imaging of the fractured string.

To standardize the stress-strain curve in ***Fig.* S7** within the elastoplastic range, an assumption was made that the in this range the volume of the strained polymer string is conserved. It is important to note that, while this principle is suitable for testing metals [1, 2] its direct application to polymers is not strictly justified. Small volume differences may arise during elongation due to the variable free volume of polymer chains or the initiation of voids at the interface between the polymer and the nanofiller. However, despite these considerations, this normalization procedure which is known as "Instantaneous Area Method" [1, 2] has proven effective and offers valuable insights, especially in the specific context of comparing the relative behavior of nanocomposite strings with varying concentrations of WS_2 nanotubes. ***Fig.* S8** exemplified this calibration procedure, displaying the measured data (continuous line), the observed UTS value, and the renormalized data (dashed lines).

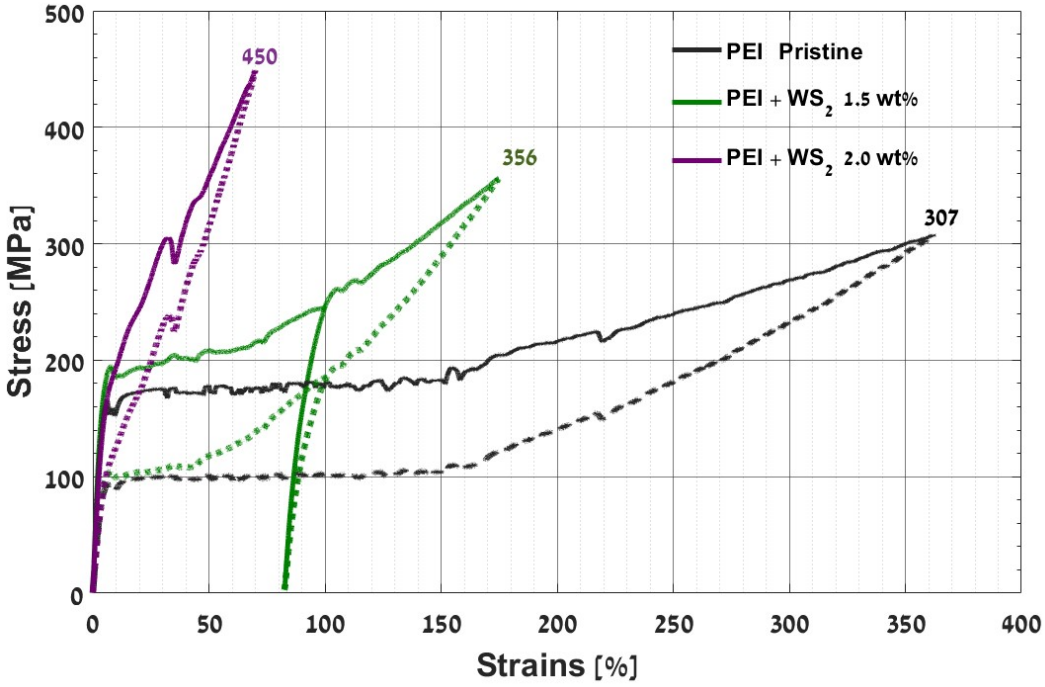

Fig. S8 - Stress-strain curves of nanocomposite strings. The continuous lines correspond to the engineering stresses as a function of the strain, and the dashed lines correspond to the true stresses after renormalizing the data.

The rescaling algorithm closely follows the principles of the "Instantaneous Area Method" [1, 2]. It commences with knowledge of the true stress value at the ultimate tensile strength (UTS) and then works backward along the entire elastoplastic range until it reaches the plateau. At this point, the cross-sectional area is considered to remain constant throughout the plateau, accounting for the non-uniform expansion of the neck. If geometrical changes obtained by elastic stretching (volume and thickness) are neglected, the cross-sectional area of the native string can be deemed as the area at both ends of the plateau. This area is used for the evaluation of the Young's modulus for the unreformed strings. Consequently, to evaluate the true stress values at any strain value (x), all that is needed to know is the applied force F_x, string length L_x, and the final cross-sectional area that attributes to the UTS when the string is broken.

eq. S1

$$True\ \sigma_x = \frac{F_x}{A_{UTS}} \cdot \frac{L_x}{L_{UTS}}$$

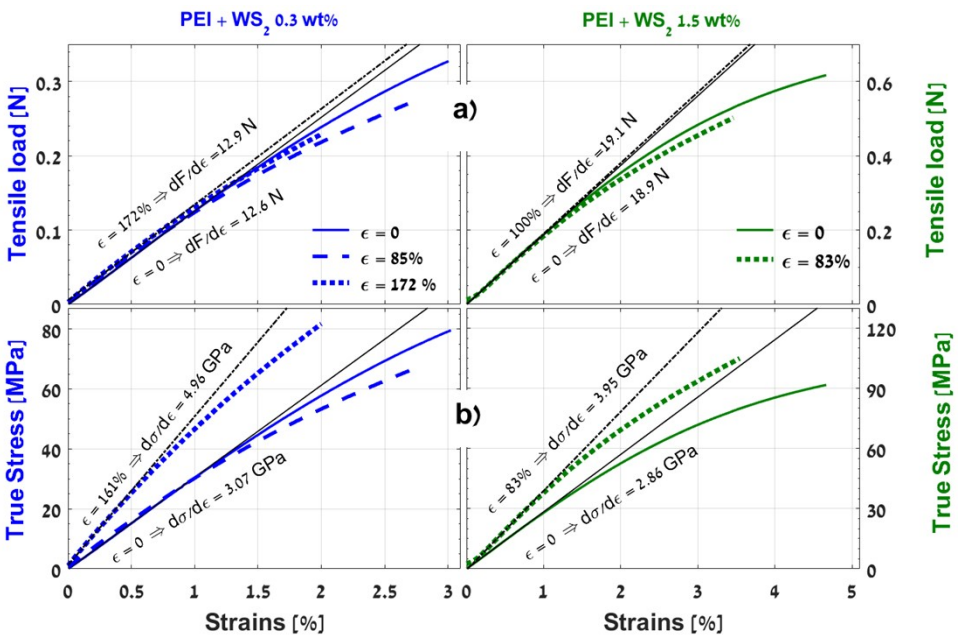

Fig. S9 - Fitted trends of (a) tensile lodes and (b) True stresses as a function of strain for the elastic segments before (native- full line) and after tensile-relaxation cycle (dashed line) measured for the nanocomposite string with 0.3 and 1.5 wt% of WS_2 INTs.

b. <u>Evidence for the reinforcement effect of the WS_2 INT</u>

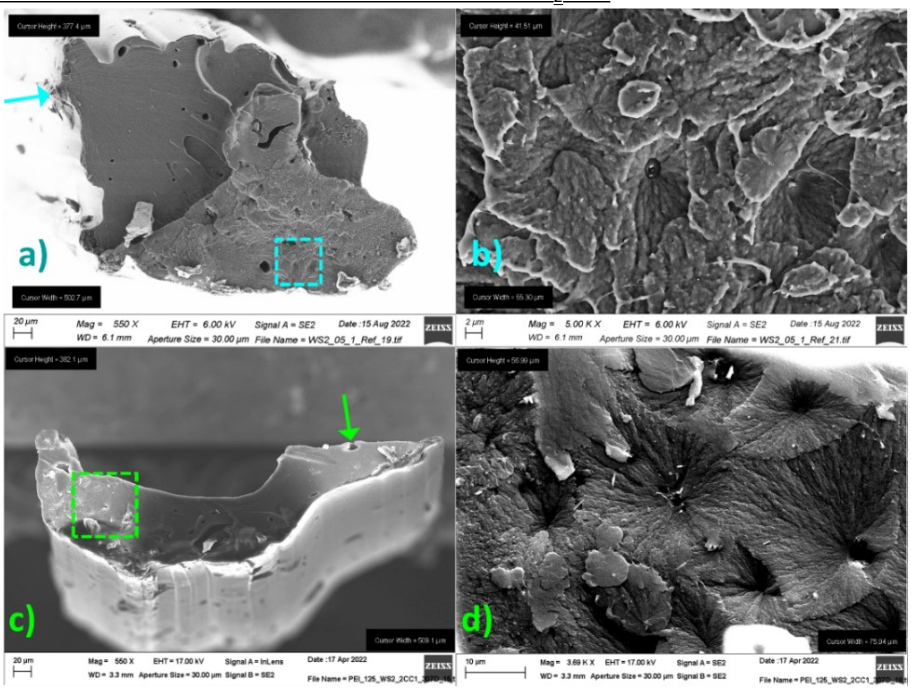

Fig. S10 - Fractured interfaces of nanocomposite strings. (a) is the image of a fractured nanocomposites string with 0.5 wt% WS_2 INT and (b) is the magnification of the cyan dashed square in (a). (c) is the image of a fractured nanocomposites string with 1.25 wt% WS_2 and (d) is the magnification of the cyan dashed square in (a). The arrows indicate the origin of the crack and the initial propagation direction.

Fig.* S10*b and ***Fig.* S10*d*** display distinct crater topography on the surface of the fractured nanocomposite strings, supporting the reinforcement achieved in the strained nanocomposite string near the WS_2 nanotubes. ***Fig.* S11** shows the deflection of propagating crack by the WS_2 nanotube.

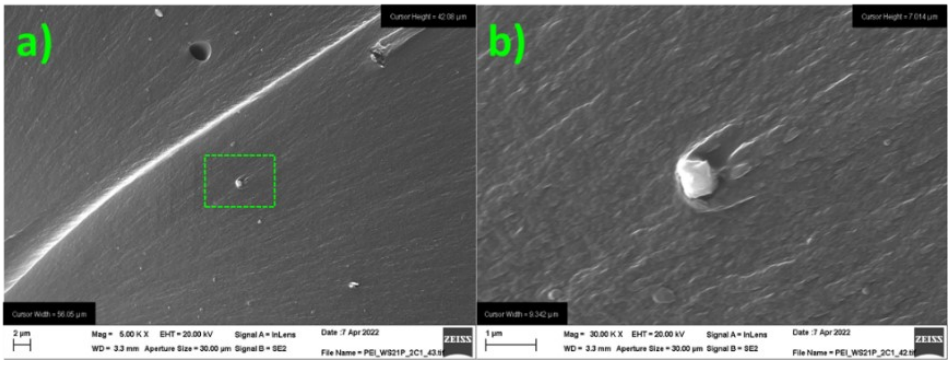

Fig. S11 - SEM image of fractured interface of a nanocomposite string. (a) A Deflection of the crack propagation direction and formation of new interfaces near the nanotube are clearly visible. (b) is the magnified image of the green-dashed square in.

c. XRD

***Fig.* S12** shows that all the native nanocomposite strings in the figure exhibit a similar broad scattering pattern, characteristic of the amorphous structure of PEI. The inset in ***Fig.* S12** shows the variation of the WS_2 (002) peak as a function of the INT content in the nanocomposite.

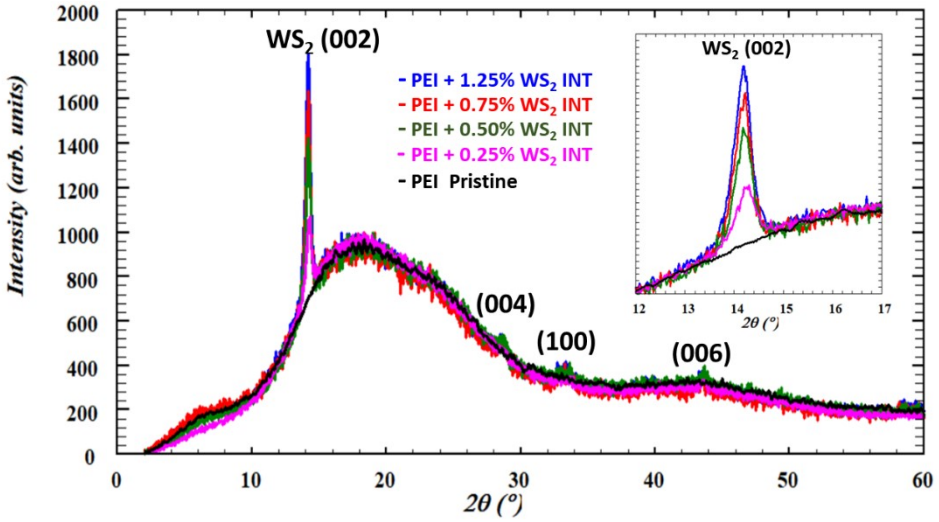

Fig. S12 - Reflection mode XRD patterns of PEI nanocomposite strings with varying fractions of WS_2 INT. The inset frame in the figure highlights the correlation between the WS_2 (002) main peak intensity (at 2θ =14.2°) and the WS_2 mass ratio in the nanocomposite blend.

d. DMA

Fig.* S13** presents the measured data of storage modulus (E'***) for the nanocomposite across the temperature range (-150 to 25°C), showing a similar trends for all the strings irrespective of the nanotubes content. ***E'*** for the pristine string is plotted across almost the entire temperature range (-120 to 250°C), showing a linear correlation between temperature and storage modulus (***E'***).

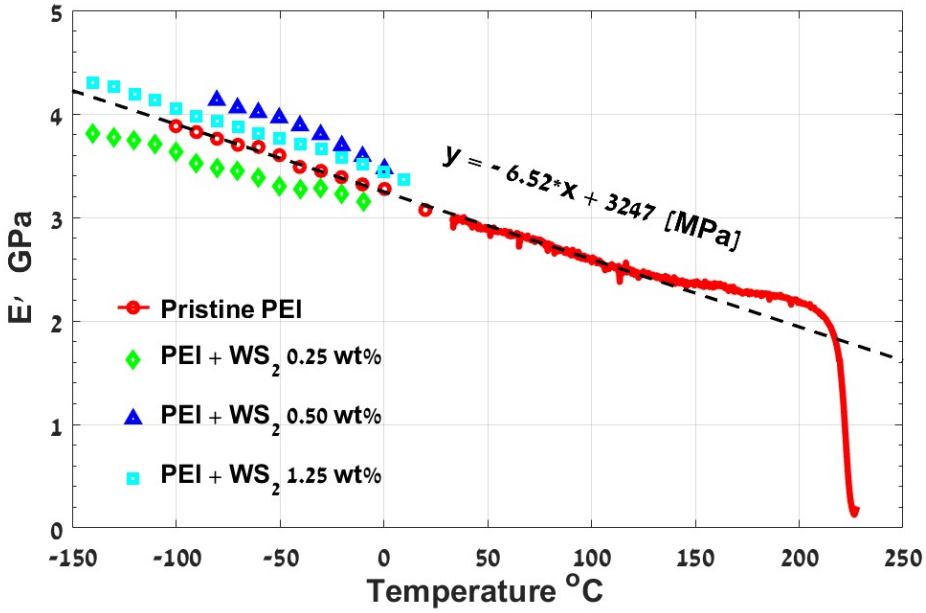

Fig. S13 - Storage modulus of the pristine and nanocomposite strings measured over a wide temperature range.

Fig.* S14** shows the normalized data of the loss modulus (E''***), storage modulus (***E'***), and their ratio, tan(δ). The normalization is done by dividing the values of each point in the curve by the value in the peak. The inset table of ***Fig.* S14** displays the values of the glass transition temperature (Tg), revealing small correlation with the WS_2 INT content in the strings.

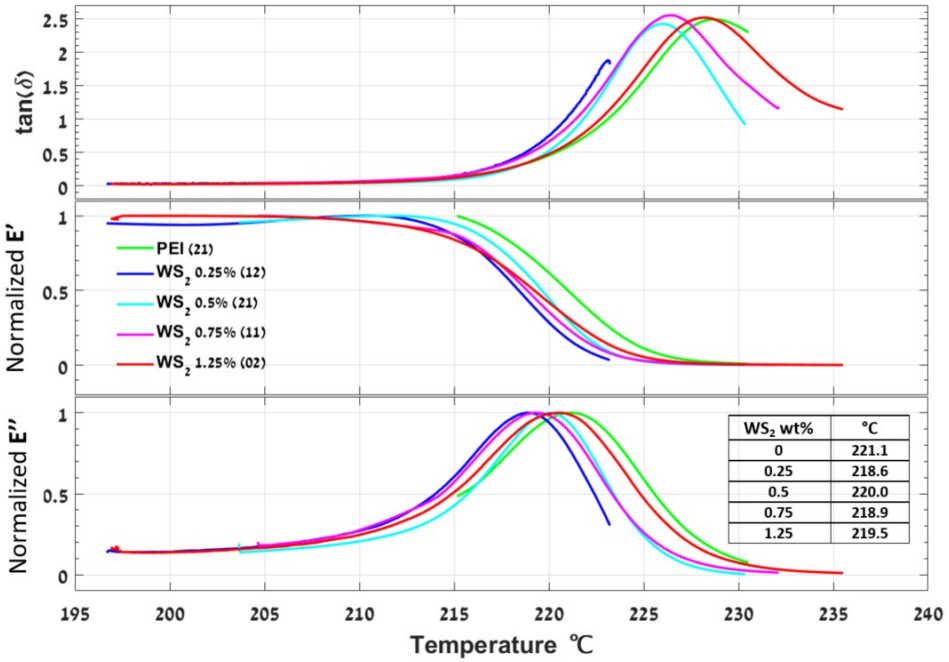

Fig. S14 – Normalized results of dynamic mechanical analysis of PEI strings with varying WS_2 INT content, including loss modulus (***E''***), storage modulus (***E'***), and tan(***δ***) ratio. Glass transition (Tg) values are listed in the inset table.

e. <u>Raman spectroscopy</u>

***Fig.* S15** illustrates the Raman spectroscopy of both the nanocomposite strings and the pristine PEI string. Notably, the distinctive peaks at 357.4 and 422.4 cm^{-1}, are characteristic of WS_2.

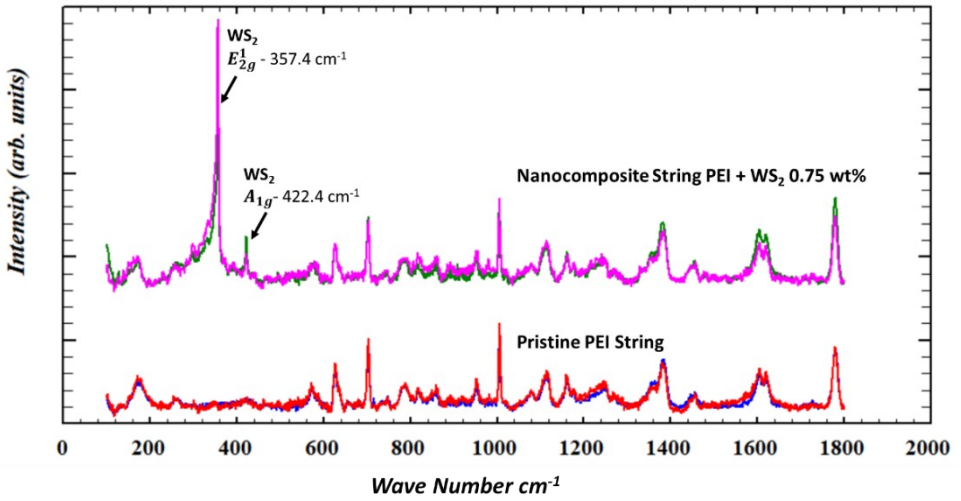

Fig. S15 - Raman spectra of individual virgin strings. The green and purple spectra were obtained from a nanocomposite string with WS_2 0.75 wt%, while the red and blue spectra represent pristine PEI strings.

***Fig.* S16** shows a comparison between Raman spectra of pristine PEI string in native (as prepared) and after it was elongated. The comparison disclosed a noticeable redshift in the vibrational mode of the vibrational mode of the meta-substituted etheric phenyl rings.

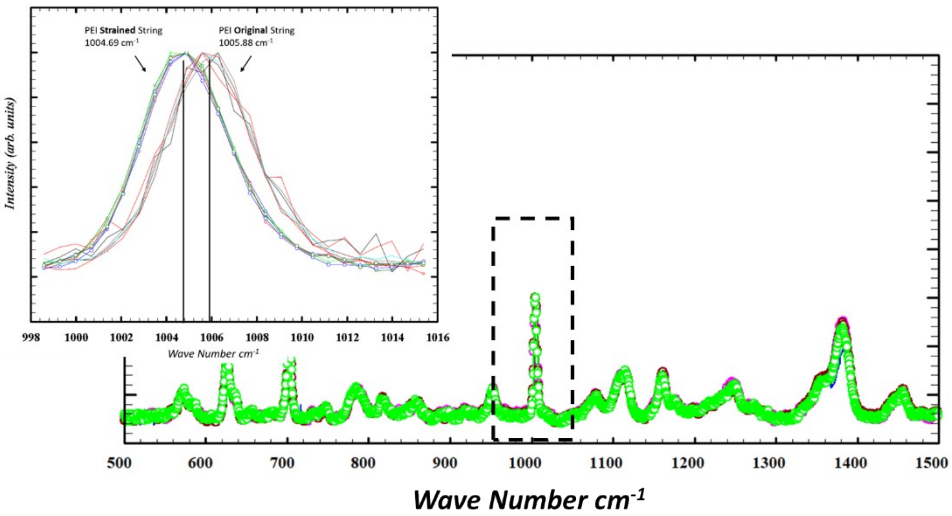

Fig. S16 – Presents the Raman spectra of pristine PEI strings before and after elongation. In the enlarged frame, the noticeable red shift of the sharp peak at 1005 cm^{-1} indicates a modification more relaxed vibrational mode of the met-substituted etheric phenyl rings.

References

[1] H. Ho, T. Xiao, C. Chen and K. Chung, "Determination of true stress strain characteristics of structural steels using Instantaneous Area Method," *Journal of Physics: Conference Series,* vol. 1777, p.

012070, 2021.

[2] D. K. Mahajan and S. Basu, "Investigations into the applicability of rubber elastic analogy to hardening in glassy polymers," *Modelling and simulation in materials science and engineering,* vol. 18, no. 2, p. 025001, 2010.